Smart Structures and Systems, *Vol. 31, No. 3 (2023) 283-299*
https://doi.org/10.12989/sss.2023.31.3.283

An Adaptive Tuned Heave Plate (ATHP) for suppressing heave motion of floating platforms

Ruisheng Ma [1a], Kaiming Bi[*2] and Haoran Zuo [3b]

[1] *Key Laboratory of Urban Security and Disaster Engineering of Ministry of Education, Beijing University of Technology, Beijing, 100124, China*
[2] *Department of Civil and Environmental Engineering, The Hong Kong Polytechnic University, Kowloon, Hong Kong, China*
[3] *Centre for Infrastructure Monitoring and Protection, School of Civil and Mechanical Engineering, Curtin University, Kent Street, Bentley, WA, 6102, Australia*

(*Received May 27, 2022, Revised January 8, 2023, Accepted February 6, 2023*)

Abstract. Structural stability of floating platforms has long since been a crucial issue in the field of marine engineering. Excessive motions would not only deteriorate the operating conditions but also seriously impact the safety, service life, and production efficiency. In recent decades, several control devices have been proposed to reduce unwanted motions, and an attractive one is the tuned heave plate (THP). However, the THP system may reduce or even lose its effectiveness when it is mistuned due to the shift of dominant wave frequency. In the present study, a novel adaptive tuned heave plate (ATHP) is proposed based on inerter by adjusting its inertance, which allows to overcome the limitation of the conventional THP and realize adaptations to the dominant wave frequencies in real time. Specifically, the analytical model of a representative semi-submersible platform (SSP) equipped with an ATHP is created, and the equations of motion are formulated accordingly. Two optimization strategies (i.e., J_1 and J_2 optimizations) are developed to determine the optimum design parameters of ATHP. The control effectiveness of the optimized ATHP is then examined in the frequency domain by comparing to those without control and controlled by the conventional THP. Moreover, parametric analyses are systematically performed to evaluate the influences of the pre-specified frequency ratio, damping ratio, heave plate sizes, peak periods and wave heights on the performance of ATHP. Furthermore, a Simulink model is also developed to examine the control performance of ATHP in the time domain. It is demonstrated that the proposed ATHP could adaptively adjust the optimum inertance-to-mass ratio by tracking the dominant wave frequencies in real time, and the proposed system shows better control performance than the conventional THP.

Keywords: adaptive tuned heave plate; heave motion reduction; inerter; offshore platforms

1. Introduction

Ocean energy is an appealing source of power with great potential and has attracted increasing attention worldwide. To harvest ocean energy, floating platforms are widely applied due to the flexible deployment and wide range of applicable water depth. In general, a floating platform is regarded as a rigid object with six degrees-of-freedom (6 DOFs), i.e., sway, surge, pitch, roll, yaw, and heave. Among the six motions, the heave motion deserves special attention since its natural frequency is normally near the dominant wave frequency, and a large heave motion can be expected due to resonance. Excessive heave motion can result in a series of adverse effects, e.g. deteriorating the operating conditions, reducing the production efficiency, and even endangering the platform safety. To this end, it is of critical importance to effectively reduce the heave motion of floating platforms.

During the past decades, researchers have devoted significant efforts to developing control systems capable of effectively reducing the heave motion of floating platforms. The originally proposed control system is the fixed heave plate (FHP), which has the following two functions: (1) provide extra damping to dissipate the vibration energy more effectively; and (2) increase the total physical mass, and thus render the heave natural frequency of platform to shift away from the dominant frequency of wave. Notably, previous experimental and numerical studies have clearly revealed the effectiveness of THP in reducing the heave motion of floating platforms (Li *et al*. 2013, Tao and Cai 2004). Nevertheless, it was also found that the FHP system might lose its control effectiveness under some extreme cases. To achieve a higher control efficiency, Liu and Ou (2016) then proposed tuned heave plate (THP), which is inspired by the tuned mass damper (TMD) widely applied in the field of civil engineering (Lu *et al*. 2021, Stewart and Lackner, 2014). The underlying principle of THP is to transfer the vibration energy of the platform within a specific frequency range to the THP system and then dissipate it. Previous studies demonstrated that the THP system is more effective in reducing undesired motions as compared to FHP (Ma *et al*. 2018, 2019). However, the THP system is found to be most effective only if it is tuned near the dominant frequency of wave (Ma *et al*. 2018). In other words, the optimum design parameters of THP, i.e.,

*Corresponding author, Ph.D., Associate Professor,
E-mail: Kaiming.bi@polyu.edu.hk
[a] Associate Professor
[b] Research Fellow

ISSN: 1738-1584 (Print), 1738-1991 (Online)

the dimensionless frequency and damping ratios, are strictly related to the external wave characteristics (i.e., the peak period and wave height) and are different for different waves. This finding is quite different from the common sense about the optimum design of tuned mass damper (TMD), namely the optimal design parameters of TMD generally depends on the structural parameters (i.e., the fundamental frequency) rather than the properties of external loads. Given that a floating platform may experience a variety of waves with different characteristics during its service life, the pre-tuned THP may be mistuned when the wave is different from the load considered during the design stage. The mistuned THP would reduce or even lose its control effectiveness, penalizing its extensive applications. From this perspective, it would be very attractive to make the THP adaptive and let it function effectively even after the change of external wave characteristics.

To date, there exist various ways to render a TMD-like system adaptive, the most common one is to implement an extra device with controllable stiffness, such as pneumatic spring (Rong and Lu 2021), magnetorheological (MR) damper (Weber and Maślanka 2012) and shape memory alloy (SMA) (Berardengo *et al*. 2015, Huang *et al*. 2020), or smart devices (Nagarajaiah and Jung 2014, Sun *et al*. 2014). However, the above devices may not be suitable for the THP due to the complexities, costs and requirements on the operating conditions. Recently, the inerter initially proposed by Smith (2002) may be an attractive alternative for developing adaptive tuned heave plate (ATHP). The inerter is a mechanical element capable of producing a resisting force proportional to the relative acceleration between its end-nodes, and the proportionality constant is generally named as "inertance". Owing to this unique property, the inerter shows two special and attractive characteristics, namely the mass amplification effect and negative stiffness effect, which unlock many possibilities for improving the conventional vibration control systems (Ma *et al*. 2021a). Specifically, the mass amplification effect refers to the fact that inerter can generate an inertance several orders of magnitude greater than its physical mass. Due to the significant mass amplification effect, inerter was widely applied to reduce the secondary mass of conventional dynamic vibration absorbers (DVAs), and various inerter-based dynamic vibration absorbers (IDVAs) were proposed, e.g. tuned inerter damper (TID) (Lazar *et al*. 2014), tuned mass-damper-inerter (TMDI) (Marian and Giaralis 2014), tuned liquid inerter system (TLIS) (Zhao *et al*. 2019), fluid inerter (Sarkar and Fitzgerald 2022), and nonlinear energy sink inerter (NSEI) (Javidialesaadi and Wierschem 2019). In previous studies, these IDVAs were demonstrated to have better control effectiveness in reducing the vibrations of various structures induced by earthquake (Pietrosanti *et al*. 2017, Song *et al*. 2021), wind (Petrini *et al*. 2020), wave (Hu *et al*. 2018, Sun and Zhang 2022) and vortex (Xu *et al*. 2020).

As for the negative stiffness effect, it specifically means that the inerter can produce a frequency-varying negative stiffness with the value of $-m_b\omega^2$, where m_b is the inertance and ω is the vibration frequency. This effect primarily endows the inerter with two applications in the field of vibration control: (1) improve the energy dissipating capacity of conventional dampers. In this aspect, many inerter-based energy dissipators have been developed, such as electromagnetic inertial mass damper (EIMD) (Nakamura *et al*. 2014, Zhu *et al*. 2019), tuned viscous mass damper (TVMD) (Ikago *et al*. 2012), rotational inertia damper (Ma *et al*. 2021b, c) and rotary eddy current damper (RECD) (Zhang *et al*. 2020); (2) enhance the performance of traditional isolators and broaden its effective frequency range (Alujević *et al*. 2018, Ma *et al*. 2020). In addition, the inerter also paves a new way for developing adaptive control systems due to the following facts: (1) the negative stiffness of inerter is highly related to its inertance, controllable negative stiffness thus can be realized by changing the inertance; (2) inerters with adjustable inertance are technologically feasible in practice and some prototypes have been developed in previous studies. In particular, Brzeski *et al*. (2017) developed and tested a novel TMD with inertance-changeable inerter, by using a continuously variable transmission (CVT) with a gear-ratio control system. It was found that the proposed control system could achieve a remarkable damping effect in a wide range of excitation frequencies. Xu *et al*. (2015) proposed a two-terminal mass (TTM) based vibration absorber with variable moment of inertia (VMI), namely TTM-VMI absorber, in which the VMI is realized via the motion of sliders embedded in a flywheel. It was demonstrated that the proposed TTM-VMI system could achieve superior control performance in many aspects. Ali Sadeghian *et al*. (2021) proposed an adaptive tuned viscous inertance damper (ATVID) that can retune itself by adjusting the inertance and damping via CVT, and analytically demonstrate its performance improvements over conventional control devices. Wang *et al*. (2018) developed a stiffness-adjustable tuned mass damper to overcome the mistuning issue of the conventional TMD, and analytically investigated its control effectiveness. The results demonstrated that the introduction of inerter could reduce the natural frequency of TMD, and lead to better control performance. Obviously, inerter provides a feasible way to develop more effective adaptive control systems, and it also sheds light on addressing the inherent issue of the conventional THP, namely the risk of mistune. However, related studies have not been reported yet.

To fill this research gap, this paper proposes an adaptive tuned heave plate (ATHP) for the heave motion reduction of floating platforms, by means of introducing a parallelly-connected inerter into the conventional THP. In this way, the proposed ATHP could be stiffness-adjustable and realize the adaptations to the dominant wave frequency in real time, overcoming the potential mistuning issue of THP. The remaining of this paper is organized as follows: Section 2 presents the negative stiffness effect of inerter; in Section 3, an analytical model of SSP-ATHP is established and validated, and two optimization strategies are formulated; Section 4 investigates the control performance of ATHP in the frequency domain, and carries out a series of parametric analyses to examine the influences of the pre-specified frequency ratio, pre-specified damping ratio, heave plate

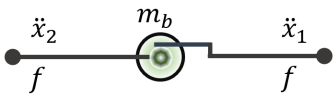

Fig. 1 Schematic drawing of inerter

sizes, peak periods and wave heights; in Section 5, a Simulink model of SSP-ATHP is constructed to study the time-domain effective of ATHP; finally, the main conclusions are drawn in Section 6.

2. Negative stiffness effect of inerter

This section discusses the negative stiffness effect of inerter, which is the basis for developing the adaptive control system proposed in the present study. Fig. 1 illustrates the schematic of inerter. As illustrated, the inerter is a two-terminal mass element, and its ideal mechanical model can be written as follows

$$f(t) = m_b[\ddot{x}_1(t) - \ddot{x}_2(t)] = m_b\ddot{x}_d(t) \tag{1}$$

in which $f(t)$ is the resisting force; t is the time; m_b is the inertance; $\ddot{x}_1$ and $\ddot{x}_2$ are the absolute acceleration of inerter at two terminals, respectively; $\ddot{x}_d$ is the relative acceleration of inerter across its two terminals.

Assuming the inerter is subjected to harmonic excitations, the force $f(t)$ can be rewritten as follows

$$f(t) = (-m_b\omega^2)Xe^{i\omega t} = K_eXe^{i\omega t} \tag{2}$$

in which ω is the vibration frequency, X is the relative displacement amplitude, and K_e is the equivalent negative stiffness. As illustrated in Eq. (2), the inerter can produce a negative stiffness with the value of $-m_b\omega^2$. In other words, the negative stiffness of inerter is determined by the inertance and the vibration frequency squared.

Fig. 2 shows the relationship between the negative stiffness and vibration frequency of inerter. For comparison, the stiffness-frequency relationships of spring and negative stiffness device (NSD) are presented as well. As shown, the negative stiffness of inerter increases exponentially with the

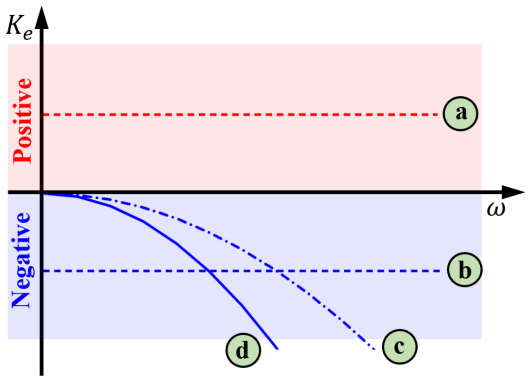

Fig. 2 Stiffness-frequency relationships of inerter, spring and NSD. (a) spring; (b) NSD; (c) small-inertance inerter; (d) large-inertance inerter

increment of the vibration frequency, and a larger inertance leads to a bigger magnitude of negative stiffness under the same vibration frequency. By contrast, the spring and NSD respectively produce constant positive and negative stiffness, which do not vary with the vibration frequency. It is also found that the negative stiffness of inerter equals to zero when the vibration frequency $\omega = 0$, indicating that the inerter does not respond to the static loads and can thus avoid the amplification of static displacement and possible instability issues. On the other hand, compared to traditional NSDs, the inerter can easily adjust its inertance by changing the diameter of the flywheel or introducing a CVT system, as mentioned in the introduction. Due to these advantages, the inerter is adopted to "retune" the conventional THP in the present study.

3. Floating platform with ATHP

3.1 Analytical model

Fig. 3 illustrates the schematic drawing of a SSP controlled by the proposed ATHP (i.e., forming a SSP-ATHP system). As shown, this adaptive control system primarily consists of buoys, a control center, a heave plate with the mass of $m_1 + m_1'$, where m_1 and m_1' are the physical and added masses of heave plate, a spring with the stiffness of k_1, a damper with the damping coefficient of c_1 and an inerter with the variable inertance $\tilde{m}_{b1}$. Notably, the added mass refers to the extra mass caused by accelerating or decelerating water around the heave plate, and the symbol "~" denotes the variant with a changeable value. To further illustrate the working principles of the proposed system, one possible implementation scheme is introduced as follows: the buoys are deployed at a certain distance away from the platform, to measure the real-time properties of the incident waves (e.g., the wave height and peak period) and transfer these data to the control center. It should be noted that the dominant wave period can be tracked by performing Fast Fourier Transform (FFT), which has been widely applied in the field of engineering, e.g., (Wang *et al*. 2007). The control center receives the data and performs optimization algorithms (e.g., genetic algorithm and pattern searching) to determine the optimum inertance value. Subsequently, the inerter adjusts its inertance accordingly to ensure the control effectiveness of ATHP under the incoming waves. It is worth mentioning that the heave plate, spring and damper of ATHP remain unchanged during this process. With such a design, the proposed ATHP can realize the purpose of the present study, i.e., adapting to the real-time wave properties.

3.1 Analytical model

Fig. 3 illustrates the schematic drawing of a SSP controlled by the proposed ATHP (i.e., forming a SSP-ATHP system). As shown, this adaptive control system primarily consists of buoys, a control center, a heave plate with the mass of $m_1 + m_1'$, where m_1 and m_1' are the physical and added masses of heave plate, a spring with the stiffness of k_1, a damper with the damping coefficient of

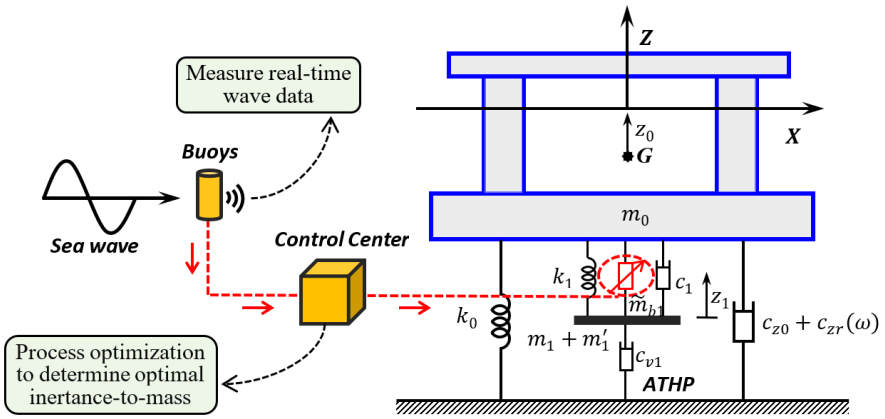

Fig.3 Schematic of the proposed SSP-ATHP system

c_1 and an inerter with the variable inertance $\tilde{m}_{b1}$. Notably, the added mass refers to the extra mass caused by accelerating or decelerating water around the heave plate, and the symbol "~" denotes the variant with a changeable value. To further illustrate the working principles of the proposed system, one possible implementation scheme is introduced as follows: the buoys are deployed at a certain distance away from the platform, to measure the real-time properties of the incident waves (e.g., the wave height and peak period) and transfer these data to the control center. It should be noted that the dominant wave period can be tracked by performing Fast Fourier Transform (FFT), which has been widely applied in the field of engineering, e.g., (Wang *et al*. 2007). The control center receives the data and performs optimization algorithms (e.g., genetic algorithm and pattern searching) to determine the optimum inertance value. Subsequently, the inerter adjusts its inertance accordingly to ensure the control effectiveness of ATHP under the incoming waves. It is worth mentioning that the heave plate, spring and damper of ATHP remain unchanged during this process. With such a design, the proposed ATHP can realize the purpose of the present study, i.e., adapting to the real-time wave properties.

According to Fig. 3, the dynamic equilibrium equations of SSP-ATHP can be written as follows

$$m_0\ddot{z}_0(t) = f_0(t) + f_{res}(t) + f_{v0}(t) + f_{rad}(t) + f_{con}(t) \tag{3a}$$

$$(m_1 + m_1')\ddot{z}_1(t) = f_1(t) + f_{v1}(t) - f_{con}(t) \tag{3b}$$

where m_Γ is the physical mass; $\ddot{z}_\Gamma(t)$ is the acceleration response; $f_\Gamma(t)$ is the wave force; $f_{v\Gamma}(t)$ is the viscous damping force. It should be noted that Γ is the label, with 0 and 1 representing the SSP and heave plate, respectively. In addition, m_1' is the added mass of the heave plate as mentioned above; $f_{res}(t)$ is the restoring force of SSP; $f_{rad}(t)$ is the radiation force acting on the SSP; $f_{con}(t)$ is the control force, which has the following form

$$f_{con}(t) = -k_1[z_0(t) - z_1(t)] - c_1[\dot{z}_0(t) - \dot{z}_1(t)] - \tilde{m}_{b1}[\ddot{z}_0(t) - \ddot{z}_1(t)] \tag{4}$$

in which k_1 is the stiffness of ATHP; c_1 is the damping coefficient of ATHP; $\tilde{m}_{b1}$ is the changeable inertance of ATHP; $z_\Gamma(t)$ and $\dot{z}_\Gamma(t)$ are the displacement and velocity, respectively.

As for the restoring force $f_{res}(t)$, it can be calculated as

$$f_{res}(t) = -k_0 z_0(t) = \rho g A_w z_0(t) \tag{5}$$

where k_0 is the restoring stiffness, which is a function of the water density ρ, gravitational acceleration g, and waterplane area A_w.

In Eq. (3), $f_{v0}(t)$ is the viscous damping force caused by the skin friction and viscous effects, and it can be expressed as follows

$$f_{v0}(t) = -c_{z0}\dot{z}_0(t) \tag{6}$$

in which c_{z0} is the damping coefficient which can be calculated according to the damping ratio measured in free-decay tests.

Besides the viscous damping force, the radiation damping force $f_{rad}(t)$ is another important damping source, which is produced by the change in the momentum of fluid during the process of platform motions. According to Cummins (1962), the radiation damping force is given byb

$$f_{rad}(t) = -m_{0\_\infty}'\ddot{z}_0(t) - \int_0^t K_0(t-t')\,\dot{z}_0(t')dt' \tag{7}$$

where $m_{0\_\infty}' = \lim_{\omega\to\infty} m_0'(\omega)$ is the added mass at infinite frequency, and $K_0(t)$ is the impulse response function of radiation.

As mentioned above, m_1 and m_1' are the physical mass and added mass of the heave plate, respectively, and they can be computed by

$$m_1 = \rho_s V \tag{8a}$$

$$m_1' = \rho c_a V_R \tag{8b}$$

in which ρ_s is the steel density; V and V_R are the physical and reference volumes of heave plate (Det Norske Veritas 2011), respectively; c_a is the added mass coefficient.

For the viscous damping force of the heave plate,

namely $f_{v1}(t)$ in Eq. (3), it can be calculated as follows

$$f_{v1}(t) = -c_{v1}\dot{z}_1(t)|\dot{z}_1(t)| \tag{9a}$$

$$c_{v1} = \frac{1}{2}\rho c_d A \tag{9b}$$

in which c_{v1} is the viscous damping coefficient; c_d is the drag coefficient of the heave plate (Det Norske Veritas 2011); A is the vertical projected area of heave plate.

Substituting Eqs. (4)-(9) into Eq. (3) gives

$$\begin{aligned}&\left(m_0 + m'_{0_\infty} + \widetilde{m}_{b1}\right)\ddot{z}_0(t) + (c_{z0} + c_1)\dot{z}_0(t)\\&+\int_0^t K_0(t-t')\,\dot{z}_0(t')dt' + (k_0 + k_1)z_0(t)\\&-\widetilde{m}_{b1}\ddot{z}_1(t) - c_1\dot{z}_1(t) - k_1 z_1(t) = f_0(t)\end{aligned} \tag{10a}$$

$$\begin{aligned}&(m_1 + m'_1 + \widetilde{m}_{b1})\ddot{z}_1(t) + c_{v1}\dot{z}_1(t)|\dot{z}_1(t)| + c_1\dot{z}_1(t)\\&+k_1 z_1(t) - \widetilde{m}_{b1}\ddot{z}_0(t) - c_1\dot{z}_0(t) - k_1 z_0(t) = f_1(t)\end{aligned} \tag{10b}$$

Obviously, Eq. (10) cannot be directly solved in the frequency domain owing to the following two nonlinear terms, namely the nonlinear viscous damping term (i.e., $c_{v1}\dot{z}_1|\dot{z}_1|$) and the convolutional term, i.e., $\int_0^t K_0(t-t')\,\dot{z}_0(t')dt'$. To calculate the frequency-domain response of SSP, the above two nonlinear terms must be firstly linearized.

According to the previous study (Chakrabarti 1987), the nonlinear viscous damping force can be linearized by

$$\dot{z}_0(t)|\dot{z}_0(t)| \approx \frac{8}{3\pi}\omega Z_0\dot{z}_0(t) \tag{11}$$

in which Z_0 is the amplitude of heave motion, which can be obtained by an iterative process.

As for the radiation force shown in Eq. (7), it can be expressed in the frequency domain as follows (Faltinsen 1993, Newman and Landweber 1978)

$$f_{rad}(s) = -m'_0(\omega)\ddot{z}_0(s) - c_{zr}(\omega)\dot{z}_0(s) \tag{12}$$

where $s = i\omega$ with i representing the imaginary unit; $m_0(\omega)$ is the frequency-dependent added mass that is caused by the fact that the vibrating floating platform can impart an acceleration to the surrounding sea water; $c_{zr}(\omega)$ is the corresponding frequency-dependent radiation damping. Generally, these parameters can be determined by using either the potential theory or existing commercial software packages. In this study, a panel model of SSP is constructed in AQWA (R17.2) to acquire the frequency-dependent coefficients. In addition, the wave force acting on SSP (i.e., f_0 in Eq. (3)) is also obtained by using the developed panel model. Notably, the wave force acting on the heave plate (i.e., f_1 in Eq. (3)) is small and thus ignored in the present study since the heave plate is assumed to be placed deep enough.

After the above linearization, Eq. (10) can be converted into the Laplace domain with the expression as follows

$$\begin{aligned}&\{[m_0 + m'_0(\omega) + \widetilde{m}_{b1}]s^2 + [c_{z0} + c_1 + c_{zr}(\omega)]s\\&+ (k_0 + k_1)\}Z_0(s)\\&-(\widetilde{m}_{b1}s^2 + c_1 s + k_1)Z_1(s) = F_0(s)\end{aligned} \tag{13a}$$

$$\begin{aligned}&[(m_1 + m'_1 + \widetilde{m}_{b1})s^2 + (c'_{v1} + c_1)s + k_1]Z_1(s)\\&-(\widetilde{m}_{b1}s^2 + c_1 s + k_1)Z_0(s) = F_1(s)\end{aligned} \tag{13b}$$

in which $Z_\Gamma(s)$ is the complex motion amplitude, and $F_\Gamma(s)$ is the complex amplitude of wave force.

For a more universal expression, the following dimensionless parameters are defined

$$\mu = \frac{m_1 + m'_1}{m_0 + m'_0(\omega)} \tag{14a}$$

$$\delta = \frac{\widetilde{m}_{b1}}{m_1 + m'_1} \tag{14b}$$

$$\gamma = \frac{\omega_1}{\omega_0} \tag{14c}$$

$$\xi_v = \frac{c_{z0}(\omega)}{2[m_0 + m'_0(\omega)]\omega_0} \tag{14d}$$

$$\xi_r = \frac{c_{zr}(\omega)}{2[m_0 + m'_0(\omega)]\omega_0} \tag{14e}$$

$$\xi_1 = \frac{c_1}{2(m_1 + m'_1)\omega_1} \tag{14f}$$

$$\xi_{v1} = \frac{c'_{v1}}{2(m_1 + m'_1)\omega_1} \tag{14g}$$

where μ is the mass ratio; δ is the inertance-to-mass ratio; ξ_v is the inherent viscous damping ratio; ξ_r is the radiation damping ratio; ξ_1 is the pre-specified damping ratio of ATHP; ξ_{v1} is the inherent damping ratio of ATHP; γ is the pre-specified frequency ratio between the SSP and ATHP; ω_0 and ω_1 are the nominal natural frequencies of the SSP and ATHP, respectively, and they can be calculated by

$$\omega_0 = \sqrt{\frac{k_0}{m_0 + m'_0(\omega)}} \tag{15a}$$

$$\omega_1 = \sqrt{\frac{k_1}{m_1 + m'_1}} \tag{15b}$$

Solving Eq. (13), the complex motion amplitudes of the SSP and heave plate can be obtained

$$Z_0(s) = \frac{A_1 A_4 + A_2 A_5}{A_3 A_1 - A_2^2} \tag{16}$$

where

$$\begin{aligned}A_1 = &(\mu + \mu\delta)s^2 + (2\mu\gamma\omega_0\xi_{v1} + 2\mu\gamma\omega_0\xi_1)s\\&+\mu\gamma^2\omega_0^2\end{aligned} \tag{17a}$$

$$A_2 = \mu\delta s^2 + 2\mu\gamma\omega_0\xi_1 s + \mu\gamma^2\omega_0^2 \tag{17b}$$

$$\begin{aligned}A_3 = &(1 + \mu\delta)s^2 + (2\omega_0\xi_v + 2\mu\gamma\omega_0\xi_1 + 2\omega_0\xi_r)s\\&+\omega_0^2 + \mu\gamma^2\omega_0^2\end{aligned} \tag{17c}$$

$$A_4 = \frac{F_0(s)}{m_0 + m_0'(\omega)} \tag{17d}$$

$$A_5 = \frac{F_1(s)}{m_0 + m_0'(\omega)} \tag{17e}$$

Subsequently, the heave response spectrum of SSP is given by

$$S_0(\omega) = S(\omega)[RAO(\omega)]^2 \tag{18}$$

where $S(\omega)$ is the JONSWAP spectrum of the incident wave, which has the following form (Chakrabarti 1987)

$$S(\omega) = a^* H_s^2 \frac{\omega^{-5}}{\omega_0^{-4}} \exp\left[-1.25\left(\frac{\omega}{\omega_0}\right)^{-4}\right] \gamma_w^{\exp\left[-\frac{(\omega-\omega_0)^2}{2\tau^2\omega_0^2}\right]} \tag{19}$$

in which ω_0 is the peak frequency of wave, H_s is the significant wave height, and

$$a^* = \frac{0.0624}{0.230 + 0.0336\gamma_w - 0.185(1.9 + \gamma_w)^{-1}} \tag{20a}$$

$$A_2 = \mu\delta s^2 + 2\mu\gamma\omega_0\xi_1 s + \mu\gamma^2\omega_0^2 \tag{20b}$$

$$\gamma_w = 3.3 \tag{20c}$$

$$\tau = \begin{cases} 0.07 & \omega \le \omega_0 \\ 0.09 & \omega > \omega_0 \end{cases} \tag{20d}$$

in which γ_w is the peakedness factor, and τ is the shape parameter.

In Eq. (18), $RAO(\omega)$ is the response amplitude operator of SSP in the heave direction, namely the ratio of the platform motion to the wave amplitude over a certain range of wave periods, and it can be computed by

$$RAO(\omega) = \frac{|Z_0(s)|}{\zeta_a} \tag{21}$$

in which ζ_a is the amplitude of wave.

As mentioned above, the heave responses of the uncontrolled SSP and the SSP controlled by the THP (SSP-THP) will also be investigated for comparison. For the complex motion amplitude of the uncontrolled SSP, it can be easily obtained by letting the parameters μ, γ, ξ_1 and δ in Eq. (16) equal to zero. Similarly, the complex motion amplitude of the SSP-THP system can be obtained by setting the parameter δ equal to zero in Eq. (16).

3.2 Optimization of ATHP

Two optimization strategies are formulated in this subsection to determine the optimum design of ATHP. For floating platforms, there exist several performance indices to quantitatively evaluate the effectiveness of the control systems, and the most concerned are the standard deviation and maximum response, and they can be expressed as follows

$$J_1 = \sqrt{\int_0^\infty S_0(\omega) d\omega} \tag{22a}$$

$$J_2 = max\,(S_0(\omega)) \tag{22b}$$

The optimization problem then becomes determining the optimum inertance-to-mass ratio δ for the given mass ratio μ, frequency ratio γ and damping ratio ξ_1 to minimize the performance indices J_n $(n = 1, 2)$ defined in Eq. (22), which is given by

$$\begin{aligned} &\textbf{minimize} \quad J_n \ (n = 1, 2) \\ &\text{subjected to} \quad \mu,\ \gamma,\ \xi_1,\ \text{and} \quad 0 \le \delta \le 8 \end{aligned} \tag{23}$$

In the present study, the inertance-to-mass ratio δ defined in Eq. (14b) is chosen as the parameter of ATHP to be optimized because the negative stiffness generated by inerter (i.e., $-m_b\omega^2$) is frequency-dependent and not constant at different frequencies. Obviously, it is very difficult to derive the exact algebraic solutions of Eq. (23) due to the frequency-dependent added mass and damping (see Eq. (12)). Therefore, a standard MATLAB® built-in genetic algorithm optimization (GA) is used to search for the optimum inertance-to-mass ratio of ATHP for all the ensuing analytical works. This genetic algorithm proved to be reliable since it has been widely used for the optimization of TMD-like control systems in many previous studies, e.g., (Kim and Kang 2012).

3.3 Prototype and validation

In this research, a classic SSP is selected as the prototype to investigate the effectiveness of using ATHP for the heave motion reduction. Fig. 4 shows the schematic drawings and detailed dimensions of the SSP. As shown,

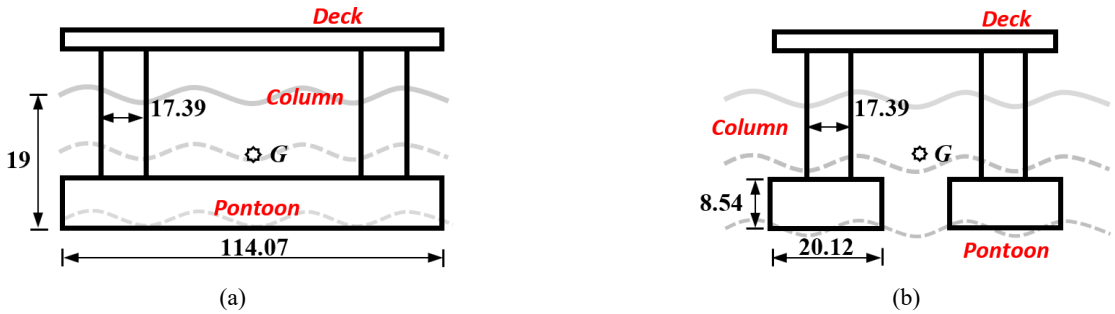

Fig. 4 Schematic drawings of SSP (m). (a) front view; (b) end view

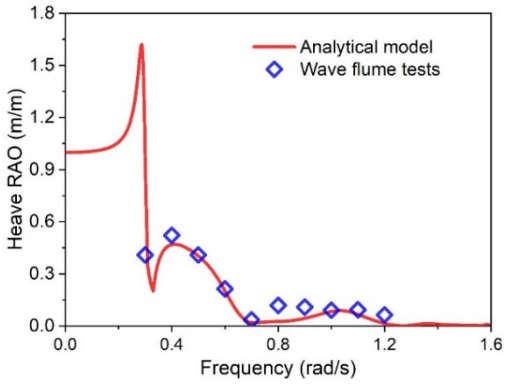

Fig. 5 Comparison on the heave RAOs obtained from the analytical model and wave flume tests (Liu and Ou 2016)

this platform mainly consists of a deck, four columns and two pontoons. The operating depth of SSP is 19 m while its physical mass reaches 51700 tonnes.

In the previous study (Liu and Ou 2016), wave flume tests were carried out for the bare SSP, i.e., the SSP without any control devices. A scaled model (1:70) of SSP was constructed, and free-decay and regular wave tests were performed. In Liu and Ou (2016), the viscous damping ratio of SSP was identified according to the results of the free-decay tests, and it was 4.48% in the heave direction. In addition, the heave RAOs of the bare SSP were also obtained by performing the regular wave tests, and the results are shown in Fig. 5. To examine the accuracy of the analytical model developed in the prior section, Fig. 5 compares the heave RAOs of the bare SSP obtained by the analytical model and wave flume tests. As shown, the RAO curve obtained by the analytical model agrees well with those acquired in the wave flume tests, demonstrating that the developed model could accurately estimate the heave motion of the selected SSP.

4. Results and discussions

This section firstly discusses the frequency-domain effectiveness of ATHP in reducing the heave motion of floating platforms. Parametric analyses are then performed to evaluate the influences of the pre-specified frequency and damping ratios, heave plate size, peak periods and wave heights on the performance of ATHP.

To quantitatively evaluate the performance improvement of ATHP over the conventional THP, a reduction ratio χ is introduced, and it can be expressed as follows

$$\chi_n = \frac{J_n(THP) - J_n(ATHP)}{J_n(THP)} \times 100\% \ (n = 1, 2) \quad (24)$$

in which $J_n(ATHP)$ and $J_n(THP)$ are the performance indexes of the SSP-ATHP and SSP-THP systems, respectively.

4.1 Control effectiveness of ATHP

This subsection investigates the effectiveness of using the proposed ATHP to reduce the heave motion of SSP. For comparison, the heave responses of the uncontrolled SSP and SSP-THP system are also calculated. Without loss of generality, a heave plate with a cross-section of 40 × 40 m is adopted in this subsection, while the wave height and peak period are chosen to be 6 m and 11 s, respectively, by referring to the previous studies (Liu and Ou 2016, Ma *et al*. 2018).

Table 1 tabulates the design parameters of the ATHP and THP systems under the given wave height and peak period. As listed, the pre-specified frequency and damping ratios of the ATHP and THP systems are respectively assumed to be 2.8 and 5% by referring to the previous studies, e.g., (Ma *et al*. 2018), and the optimum inertance-to-mass ratios of ATHP determined by J_1 and J_2 optimizations are 0.840 and 0.988, respectively. It should be noted that the pre-specified frequency ratios of the ATHP and THP are greater than 1.0, which seems to contradict the common sense that the optimal frequency ratio of the traditional TMD is generally around unity to assure that the TMD resonates with the superstructure and thus dissipates more vibration energy. The reason is that the heave natural periods of floating platforms are required to fall outside the dominant wave energy range to avoid any possible catastrophic resonance during the stage of design. Generally, the heave natural period of a floating platform is larger than 20 s while the wave peak period ranges 6~14 s (Det Norske Veritas 2011). To achieve the best control performance, the THP should be tuned near the dominant wave period rather than the natural period of SSP, the pre-specified frequency ratio defined in Eq. (14c) is thus greater than 1.0. Parametric studies will be performed later to investigate the influence of the pre-specified frequency and damping ratios.

Fig. 6 shows the comparison between the heave response spectra of the SSP controlled by the ATHP and THP. Notably, the heave response spectrum of the uncontrolled SSP is also presented for comparison. Some general information can be obtained from the figure: (1) both the ATHP and THP can effectively reduce the heave motion of SSP compared to the uncontrolled SSP; (2) the proposed ATHP shows better performance than the

Table 1 Design parameters of ATHP and THP

Control systems	Optimizations	Pre-specified frequency ratio γ	Pre-specified damping ratio ξ_1	Inertance-to-mass ratio δ
THP	NA	2.8	5%	NA
ATHP	J_1	2.8	5%	0.840
ATHP	J_2	2.8	5%	0.988

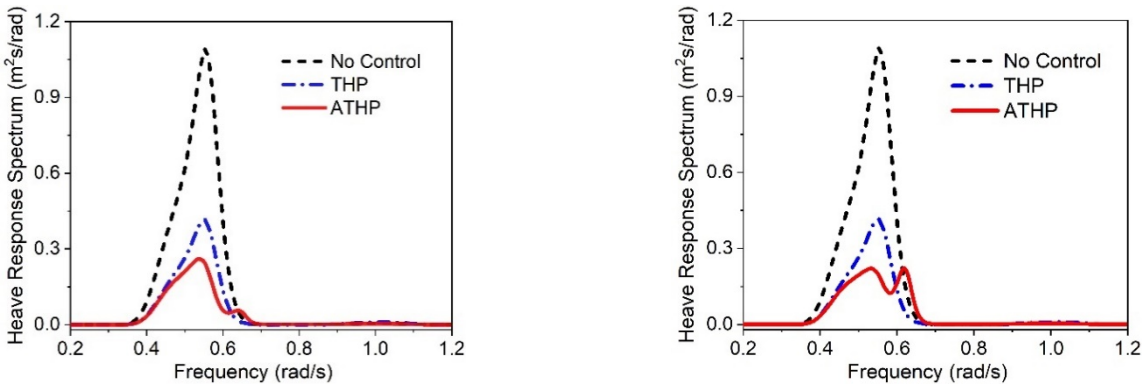

Fig. 6 Comparison between the heave response spectra of SSP without control and controlled by ATHP and THP. (a) J_1 optimization; (b) J_2 optimization

Table 2 Performances and reduction ratios of ATHP

Performances	THP	ATHP	Reduction ratio χ_1/χ_2 (%)
J_1	0.228	0.194	15.20
J_2	0.416	0.222	46.64

conventional THP. As listed in Table 2, χ_1 and χ_2 attain 15.20% and 46.64%, respectively; (3) both J_1 and J_2 optimizations are valid for searching the optimum inertance-to-mass ratio of ATHP. It is also found that the heave response spectrum of the uncontrolled SSP shows a one-peak characteristic, and the peak appears around 0.57 rad/s, corresponding to the peak period of the selected wave. By introducing the ATHP and THP systems, the peak of the heave response spectrum of the uncontrolled SSP around 0.57 rad/s can be significantly reduced. Specifically, For the SSP-THP system, the heave response spectrum also shows the one-peak characteristic. However, the heave response spectrum of the SSP-ATHP system has a major peak under J_1 optimization and two roughly equal peaks under J_2 optimization. This phenomenon can be attributed to the difference between J_1 and J_2 performances defined in Eq. (22): J_1 optimization focuses on reducing the heave response over the entire frequency range while J_2 optimization is concerned with mitigating the maximum heave response of SSP. These results are similar to those of ordinary TMD under H_2 and H_∞ optimizations (Asami *et al*. 2002).

4.2 Influences of pre-specified frequency and damping ratios

In this subsection, the influences of the pre-specified frequency and damping ratios on the control performance of ATHP are discussed. Similarly, a 40 × 40 m heave plate is adopted for ATHP, and the wave height and peak period are set as 6 m and 11 s, respectively. The following two schemes are considered: (1) the pre-specified frequency ratio of ATHP increases from 2.5 to 3.2 with an increment of 0.1 while the pre-specified damping ratio is kept at 5%; (2) the pre-specified damping ratio of ATHP increases from 1% to 8% with an increment of 1% while the pre-specified frequency ratio is kept at 2.8. It should be noted that the same schemes are also considered for the pre-specified frequency and damping ratios of THP.

Fig. 7 shows the optimum inertance-to-mass ratios of ATHP with different pre-specified frequency and damping ratios. As shown in Fig. 7(a), both the optimum inertance-to-mass ratios of ATHP under J_1 and J_2 optimizations increase almost linearly with the increment of pre-specified frequency ratio. This is because a larger negative stiffness is required when the pre-specified eigenfrequency of ATHP shifts farther from the dominant wave frequency. Fig. 7(b) shows the influence of the pre-specified damping ratio on the optimum inertance-to-mass ratio of ATHP. As illustrated, the optimum inertance-to-mass ratio under J_1 optimization firstly increases with the increment of pre-specified damping ratio, and then tends to be constant when the pre-specified damping ratio exceeds 4%. As for J_2, the optimum inertance-to-mass ratio increases with the growth of pre-specified damping ratio. However, the increasing extent decreases slightly when the pre-specified damping ratio is larger than 4%. The different varying trends of the optimum inertance-to-mass ratios under J_1 and J_2 optimizations can be primarily attributed to the discrepancies in the objective functions of these two optimizations. As discussed above, J_1 optimization focuses on reducing the heave response over the entire frequency range while J_2 optimization is concerned with mitigating the maximum heave response of SSP. Moreover, the optimum inertance-to-mass ratio of ATHP under J_2 optimization is larger than that under J_1 optimization at a given pre-specified frequency or damping ratio. In other words, a larger inertance is generally required for the ATHP system under J_2 optimization. Furthermore, the optimum inertance-to-mass ratio of ATHP is found to be sensitive to the variation of the pre-specified frequency ratio, while relatively insensitive to the variation of the pre-specified damping ratio. Similar results were also reported for the THP system in a previous study (Ma *et al*. 2019).

Fig. 8 shows the influences of the pre-specified frequency and damping ratios on the reduction ratios of ATHP. As shown in Fig. 8(a), both χ_1 and χ_2 firstly increase and then decrease with the increase of pre-

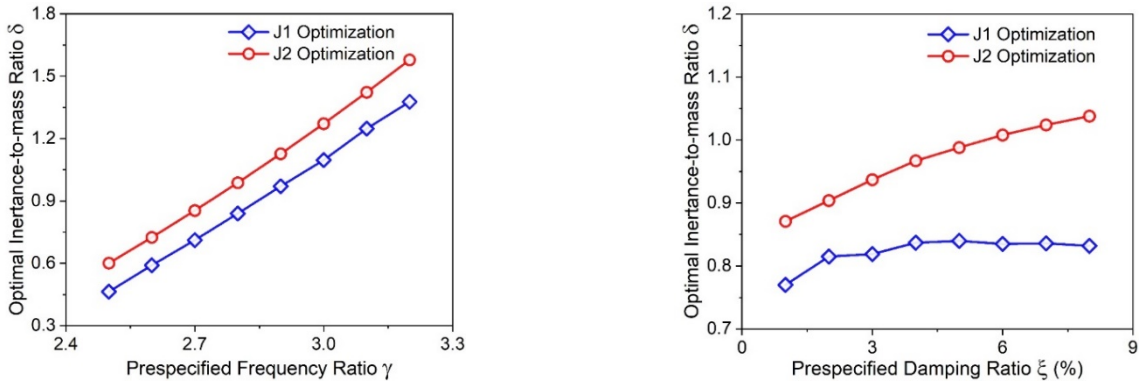

(a) (b)

Fig. 7 Influence of the pre-specified frequency and damping ratios on the optimum inertance-to-mass ratios of ATHP. (a) pre-specified frequency ratio ($\xi = 5\%$); (b) pre-specified damping ratio ($\gamma = 2.8$)

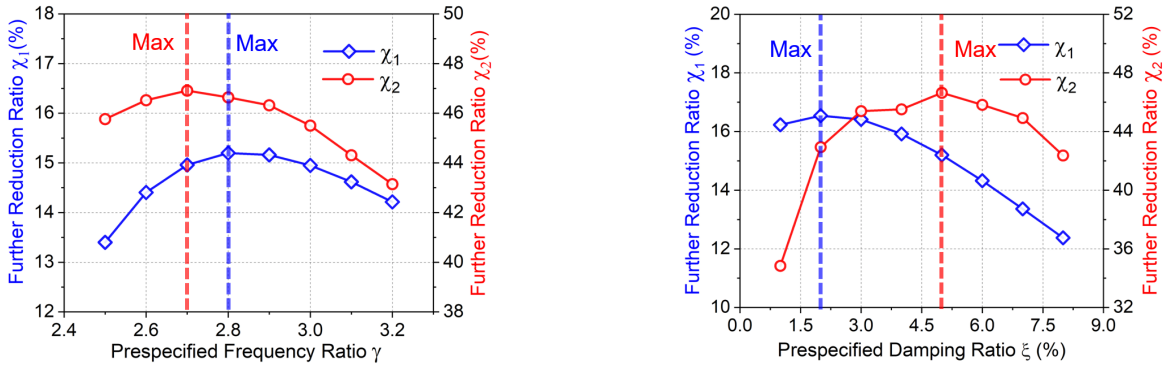

(a) (b)

Fig. 8 Influence of pre-specified frequency and damping ratios on the reduction ratios of ATHP. (a) pre-specified frequency ratio ($\xi = 5\%$); (b) pre-specified damping ratio ($\gamma = 2.8$)

specified frequency ratio γ, so that a maximum value exists in each curve. In particular, the maximum value of χ_1 is 15.20% at the pre-specified frequency ratio of 2.8, and the maximum value of χ_2 is 46.91% at the pre-specified frequency ratio of 2.7. Fig. 8(b) displays the influence of the pre-specified damping ratio on the reduction ratios of ATHP. Similarly, both χ_1 and χ_2 initially increase and then decrease with the growth of pre-specified damping ratio. The maximum value of χ_1 is 16.54% at the pre-specified damping ratio of 2% while the maximum value of χ_2 is 46.64% at the pre-specified damping ratio of 5%. Obviously, for a given wave with a specific peak period and wave height, there exists optimum pre-specified frequency and damping ratios to let the ATHP achieve the best performance improvement, and J_1 and J_2 optimizations result in different optimum values.

4.3 Influence of heave plate sizes

To evaluate the influence of heave plate size on the effectiveness of ATHP, five heave plates with the size ranging from 30×30 m to 50×50 m are considered in this subsection. A wave with a height of 6 m and a peak period of 11 s is chosen as the input, and the pre-specified frequency and damping ratios are assumed as 2.8 and 5%, respectively.

Fig. 9(a) shows the influence of the heave plate size on the optimum inertance-to-mass ratio of ATHP. As shown, the optimum inertance-to-mass ratio of ATHP under J_1 optimization slightly increases from 0.795 to 0.875 as the heave plate size increases from 30×30 m to 50×50 m. As for J_2 optimization, the optimum inertance-to-mass ratio of ATHP slightly decreases first and then increases with the increase of heave plate size, and the minimum value of δ is observed when the plate size is 40×40 m. It should be noted that the differences between the maximum and minimum values of δ under J_1 and J_2 optimizations are respectively 0.08 and 0.042, which are 9.1% and 4.1% of the maximum values. This fact indicates that the heave plate sizes have a limited influence on the optimum inertance-to-mass ratio of ATHP. Moreover, compared to J_2 optimization, J_1 optimization is found to require a smaller inertance-to-mass ratio when the same heave plate is used, which is consistent with the results observed in Section 4.1.

Table 3 tabulates the performance indexes and corresponding reduction ratios of the ATHP with different plate sizes, and Fig. 9(b) shows the relationship between the reduction ratio and heave plate size. Both χ_1 and χ_2 increase almost linearly with the increment of the heave

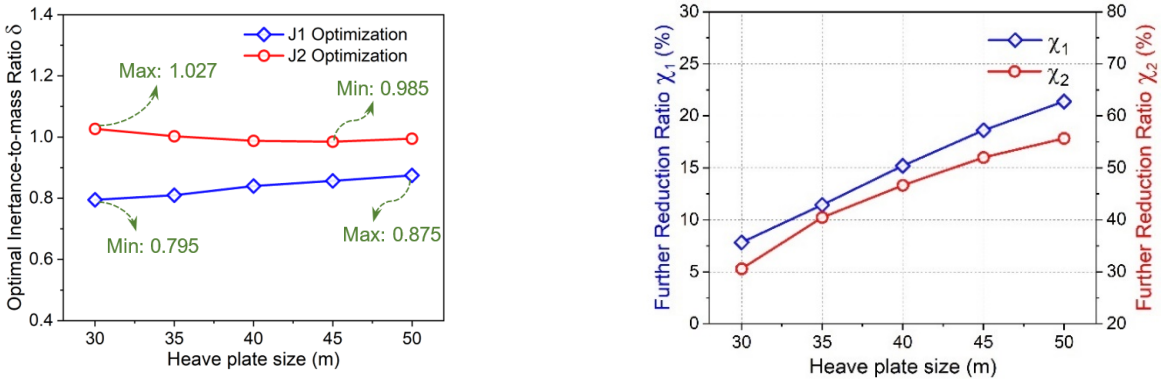

(a) (b)

Fig. 9 Influence of heave plate size ($\gamma = 2.8,\ \xi = 5\%$): (a) optimum inertance-to-mass ratio; and (b) reduction ratios

Table 3 Performance indexes and reduction ratios of ATHP with different plate sizes

Performances	Control systems	Plate sizes (m × m)				
		30 × 30	35 × 35	40 × 40	45 × 45	50 × 50
J_1	THP	0.288	0.258	0.228	0.199	0.172
	ATHP	0.265	0.229	0.194	0.162	0.135
	$\chi_1(\%)$	7.83	11.43	15.20	18.61	21.38
J_2	THP	0.674	0.540	0.416	0.312	0.229
	ATHP	0.468	0.321	0.222	0.150	0.101
	$\chi_2(\%)$	30.59	40.45	46.64	51.99	55.66

plate size. In other words, a larger heave plate size can lead to a better performance improvement of ATHP. For example, the reduction ratio χ_1 of the 50×50 m ATHP is nearly three times of the 30×30 m ATHP. Therefore, it can be concluded that the heave plate size has a significant influence on the control performance of ATHP.

4.4 Influence of peak periods

In this subsection, the control effectiveness of ATHP subjected to the waves with different peak periods is investigated. As discussed in Section 4.3, the reduction ratio of ATHP is proportional to the heave plate size, a heave plate with the size of 50×50 m is thus chosen in this subsection. Similarly, the pre-specified frequency and damping ratios of the ATHP and THP are set to be 2.8 and 5%, respectively. It is worth noting that the wave peak period increases from 6 s to 14 s with an increment of 1 s, while the wave height remains at 6 m.

Fig. 10 shows the influence of different peak periods on the optimum inertance-to-mass ratio of ATHP. For convenience, the entire wave period range is divided into two ranges, namely Range A (T $\leq$ 7.6 s) and Range B (T $>$ 7.6 s). It should be noted that the demarcation line between Ranges A and B (i.e., the dashed green line in the figure) corresponds to the initial natural period of ATHP, which can be calculated by the pre-specified frequency ratio. Interestingly, all the optimum inertance-to-mass ratios in Range A are equal to zero no matter which optimization method is used. This is because the ATHP is developed

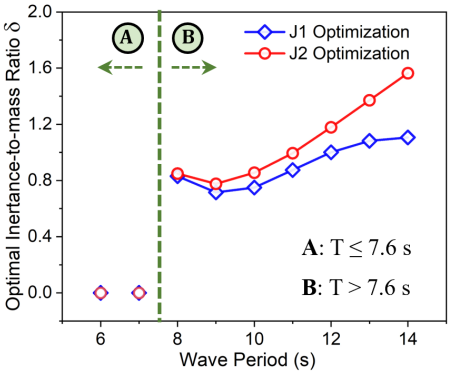

Fig. 10 Influence of wave peak periods on the optimum inertance-to-mass ratios of ATHP ($\gamma = 2.8,\ \xi = 5\%$)

based on the negative stiffness effect of inerter and can be retuned only when its initial natural period is less than the wave peak period. When the initial natural period of ATHP is larger than the wave peak period, the negative stiffness provided by inerter would become zero since adding the negative stiffness in this case could further shift the initial natural period of ATHP away from the wave peak period and thus degrade the control effectiveness. This is the reason why the optimum inertance-to-mass ratios of ATHP are equal to zero in Range A (T $\leq$ 7.6 s). In Range B, the optimum inertance-to-mass ratios under J_1 and J_2 optimizations generally increase with the increment of the

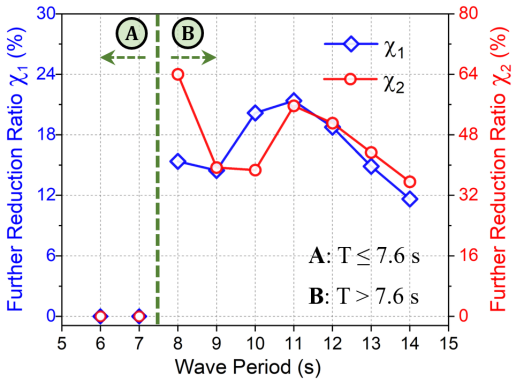

Fig. 11 Influence of wave peak periods on the reduction ratios of ATHP ($\gamma = 2.8$, $\xi = 5\%$)

wave peak period except those at the peak period of 8 s. This can be attributed to the fact that the farther the wave peak period shifts away from the initial natural period of ATHP, the larger is the required negative stiffness (i.e., the inertance-to-mass ratio) to retune the control system. Moreover, the optimum inertance-to-mass ratios of ATHP under J_1 optimization are found to be less than those under J_2 optimization when the SSP is subjected to the wave with the same peak period, which agrees with the finding in Sections 4.1, 4.2 and 4.3. Furthermore, the increasing extent of the optimum inertance-to-mass ratio deceases with the increase of the wave peak period under J_1 optimization especially when the wave peak period exceeds 12 s, while no such trend is observed for J_2 optimization.

Table 4 lists the performances and reduction ratios of the ATHP when the SSP is subjected to the waves with different peak periods, and Fig. 11 shows the relationship between the reduction ratio and the wave peak period. Similarly, the entire wave period range is also divided into Ranges A and B. As shown, χ_1 and χ_2 in Range A are equal to zero, indicating that the ATHP has the same control performance as the THP. This is because the optimum inertance-to-mass ratios of ATHP in Range A are zero (see Fig. 10), and the ATHP would thus behave like a conventional THP. In Range B, no clear overall trend can be found, and the maximum values of χ_1 and χ_2 are observed at the peak periods of 11 s and 8 s, respectively. However, if the results at the peak period of 8 s are excluded, both χ_1 and χ_2 roughly show the trend of an increase followed by a decrease, and both the maximum values of χ_1 and χ_2 appear at the peak period of 11 s. To illustrate the above findings, Fig. 12 displays the heave response spectra of the uncontrolled SSP, SSP-ATHP and SSP-THP systems subjected to the waves with different peak periods. It should be noted that only the heave response spectra at the peak periods of 8 s, 11 s, and 14 s are presented for conciseness. Some general conclusions can be drawn: (1) both the ATHP and THP are effective in reducing the heave response spectra of the uncontrolled SSP around the highest peak; (2) the ATHP is more effective than the conventional THP in reducing the heave motion. When the peak periods are 11 s and 14 s, the heave response spectra of the SSP-THP system show a one-peak characteristic while the heave response spectra of the SSP-ATHP system show one main peak under J_1 optimization and two approximately equal peaks under

Table 4 Performances and reduction ratios of ATHP subjected to waves with different peak periods

Performances	Wave height (m)	Peak period (s)	Control systems		Reduction ratio χ_1/χ_2(%)
			THP	ATHP	
J_1	6	6	0.127	0.127	0
	6	7	0.089	0.089	0
	6	8	0.073	0.062	15.37
	6	9	0.084	0.072	14.47
	6	10	0.120	0.096	20.16
	6	11	0.172	0.135	21.38
	6	12	0.219	0.178	18.76
	6	13	0.253	0.215	14.88
	6	14	0.272	0.240	11.64
J_2	6	6	0.131	0.131	0.00
	6	7	0.045	0.045	0.00
	6	8	0.029	0.010	64.00
	6	9	0.031	0.019	39.35
	6	10	0.078	0.048	38.67
	6	11	0.229	0.101	55.66
	6	12	0.445	0.218	51.10
	6	13	0.643	0.364	43.32
	6	14	0.785	0.506	35.58

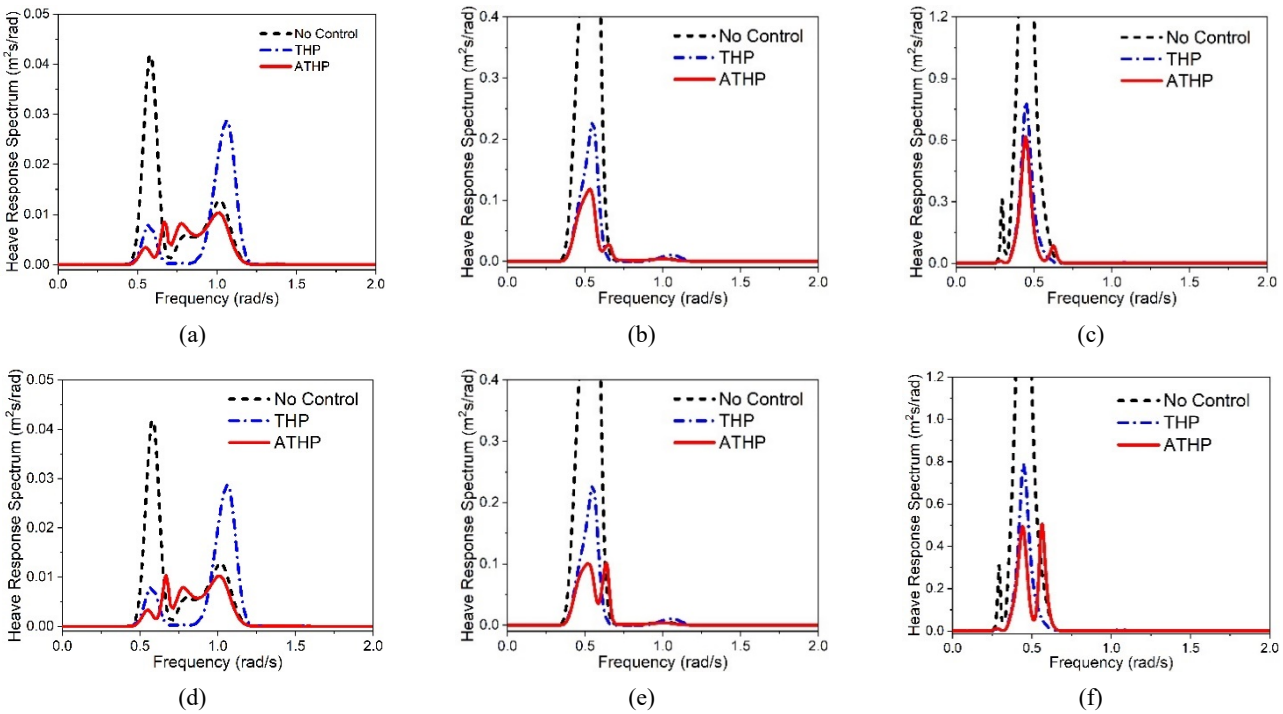

Fig. 12 Heave response spectra of SSP subjected to waves with different peak periods. (a) T = 8 s, J_1 optimization; (b) T = 11 s, J_1 optimization; (c) T = 14 s, J_1 optimization; (d) T = 8 s, J_2 optimization; (e) T = 11 s, J_2 optimization; (f) T = 14 s, J_2 optimization

J_2 optimization, as shown in Figs. 12(b), (c), (e) and (f), respectively. However, the heave response spectra of the uncontrolled SSP, SSP-ATHP and SSP-THP show some different characteristics when the peak period is 8 s (see Figs. 12(a) and (d)). The differences primarily include: (1) besides the main peak around 0.58 rad/s, the heave response spectrum of the uncontrolled SSP has another obvious peak at a higher frequency (around 1 rad/s); (2) the THP seriously aggravates the heave response of SSP in the frequency range of 0.95~1.2 rad/s although it effectively suppresses the heave response of SSP around 0.45~0.95 rad/s; (3) more than three obvious peaks can be observed in the heave response spectra of SSP-ATHP no matter which optimization method is used. These differences are the direct reasons why the reduction ratios at the peak period of 8 s, especially under J_2 optimization do not follow the overall trend in Fig. 11. In general, the wave peak period has a significant influence on the optimum inertance-to-mass ratio and performance improvement of the proposed ATHP system.

4.5 Influence of wave heights

This subsection examines the influence of wave height on the control effectiveness of ATHP. Similar to Section 4.4, a heave plate with the size of 50×50 m is selected and the pre-specified frequency and damping ratios of the ATHP and THP systems are 2.8 and 5%, respectively. Notably, the wave height increases from 2 m to 10 m with an increment of 1 m while the wave peak period is kept at 11 s.

Fig. 13 illustrates the optimum inertance-to-mass ratios of ATHP subjected to the waves with different heights. As

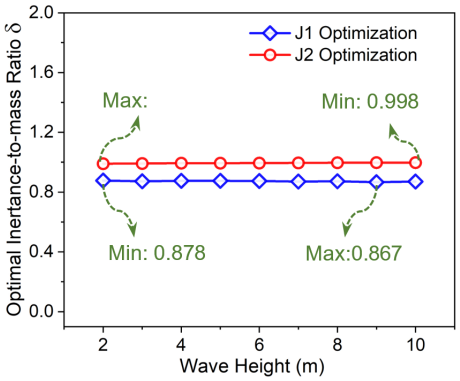

Fig. 13 Influence of wave height on the optimum inertance-to-mass ratios of ATHP ($\gamma = 2.8$, $\xi = 5\%$)

illustrated, the wave height has a very marginal influence on the optimum inertance-to-mass ratio of ATHP no matter which optimization method is used. For example, the maximum and minimum values of δ under J_2 optimization are 0.991 and 0.998, respectively, and the difference between the maximum and minimum values is only 0.7%. Table 5 lists the performances and reduction ratios, and Fig. 14 shows the relationship between the reduction ratio and the wave height. As shown, both the reduction ratio curves (i.e., χ_1 and χ_2) are almost straight lines with very small slope, indicating that the wave height has a negligible influence on the reduction ratio of ATHP. It is reasonable to conclude that the influence of wave height on the optimum inertance-to-mass ratio and control

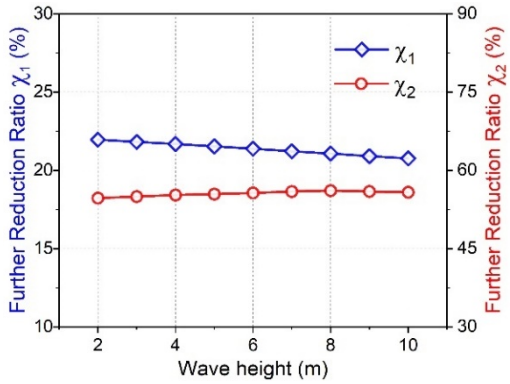

Fig. 14 Influence of wave height on the reduction ratios of ATHP (γ = 2.8, ξ = 5%)

effectiveness of ATHP can be neglected.

5. Time-domain realization of ATHP

In Section 4, the control effectiveness of ATHP is demonstrated in the frequency domain and parametric analyses are performed to evaluate the influences of various parameters. This section realizes the ATHP in the time domain by developing a Simulink model in MATLAB (R2017a) and investigates the time-domain control effectiveness of ATHP. Fig. 15 shows the developed Simulink model, which consists of three parts, namely the SSP, ATHP and control center, which are displayed in red, blue and green, respectively. In particular, the SSP part primarily includes four feedback loops, namely the restoring force with respect to displacement (k_0), the radiation damping force with respect to velocity (the state-space block in the figure), the viscous force with respect to velocity (c_{z0}), and the control force produced by ATHP (f_{con}). The ATHP part also includes four feedback loops, which are the elastic force with respect to the relative displacement (k_1), the damping force with respect to the relative velocity (c_1), the inertial force with respect to the relative acceleration ($\widetilde{m}_{b1}$) and the nonlinear damping force with respect to the squared velocity (c_{v1}). As for the control center, it deals with the real-time data transferred from the buoys (see Fig. 2), and then outputs the optimum inertance-to-mass ratio ($\widetilde{m}_{b1}$) to the ATHP. It is worth mentioning that: (1) as discussed in Section 4, the peak period can significantly affect the optimum inertance-to-mass ratio of ATHP while the wave height has a negligible effect. Therefore, the inertance-to-mass ratio of ATHP is optimized and determined only according to the wave peak period; (2) for simplicity purposes, possible time lags from signal processing are not considered in the Simulink model.

In Fig. 15, the total masses of SSP and ATHP (i.e., M_0 and M_1) can be calculated as follows

$$M_0 = m_0 + m'_{0\_\infty} \tag{25a}$$

$$M_1 = m_1 + m'_1 \tag{25b}$$

Moreover, the radiation damping force is time-consuming to solve due to the existence of the convolutional term in Eq. (7), namely $\int_0^t K_0(t-t')\dot{z}_0(t')dt'$. For this reason, an equivalent state-space model is introduced as follows

Table 4 Performances and reduction ratios of ATHP subjected to waves with different peak periods

Performances	Wave height (m)	Peak period (s)	Control systems		Reduction ratio χ_1/χ_2(%)
			THP	ATHP	
J_1	2	11	0.057	0.045	21.97
	3	11	0.086	0.067	21.82
	4	11	0.115	0.090	21.68
	5	11	0.143	0.112	21.53
	6	11	0.172	0.135	21.38
	7	11	0.200	0.158	21.23
	8	11	0.229	0.181	21.07
	9	11	0.258	0.204	20.92
	10	11	0.286	0.227	20.76
J_2	2	11	0.025	0.011	56.45
	3	11	0.057	0.025	56.24
	4	11	0.102	0.045	55.71
	5	11	0.159	0.070	55.88
	6	11	0.229	0.101	55.66
	7	11	0.311	0.139	55.51
	8	11	0.407	0.182	55.23
	9	11	0.515	0.232	54.99
	10	11	0.635	0.284	55.23

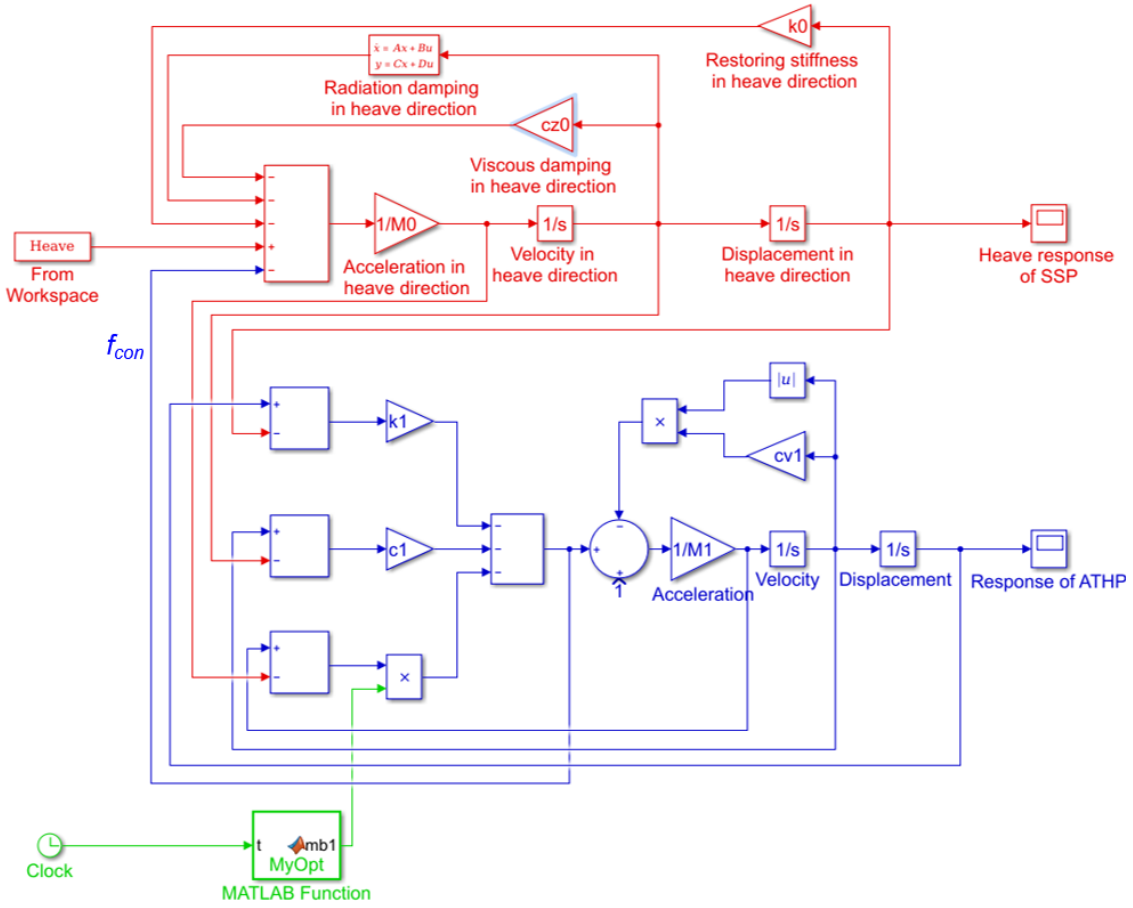

Fig. 15 Simulink model of the SSP controlled by ATHP

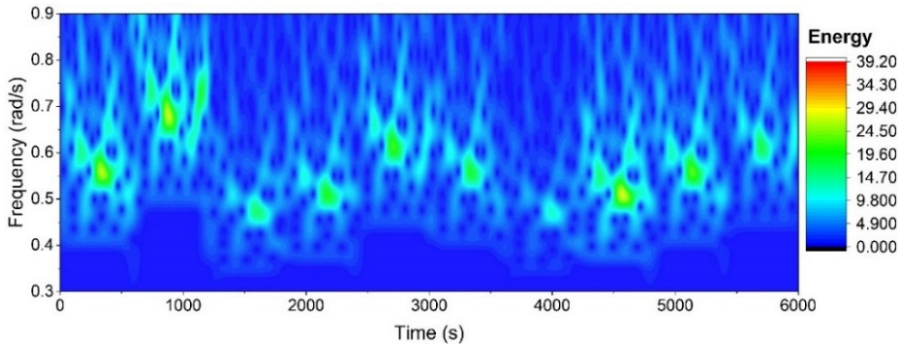

Fig. 16 Wavelet transform of wave elevation

$$\begin{cases} \dot{\boldsymbol{x}}(t) = \boldsymbol{A}\boldsymbol{x}(t) + \boldsymbol{B}\dot{z}_0(t) \\ y(t) = \boldsymbol{C}\boldsymbol{x}(t) \approx \int_0^t K_0(t-t')\,\dot{z}_0(t')dt' \end{cases} \tag{26}$$

where $\dot{z}_0(t)$ and $y(t)$ are the input and output of system at time t; $\boldsymbol{x}$ is the state vector; $\boldsymbol{A}$, $\boldsymbol{B}$, and $\boldsymbol{C}$ are the system matrices. It should be noted that the toolbox developed in (Perez and Fossen, 2009) is used to identify the parameters in Eq. (26) and the infinite-frequency added mass (i.e., m'_{0_∞} in Eq. (25)). As for the other parameters in Fig. 15, they are the same as those defined in Section 3.

Without loss of generality, a heave plate with the size of 50 × 50 m is adopted for the ATHP in the Simulink model while the pre-specified frequency and damping ratios are selected as 2.8 and 5% respectively again. Moreover, an artificial sea wave with a duration of 6000 s is generated as the input excitation by using ANSYS AQWA mentioned in Section 3. Fig. 16 shows the wavelet transform of the wave elevation. As shown, both the dominant frequency and energy of wave vary with time. It should be noted that an interval of 600 s is chosen in the Simulink model to update the ATHP, i.e., adjust the inertance-to-mass ratio in the system.

Fig. 17 illustrates the heave motion time histories of the SSP controlled by the ATHP and the time-varying inertance-to-mass ratio of ATHP (i.e., the solid purple lines in the

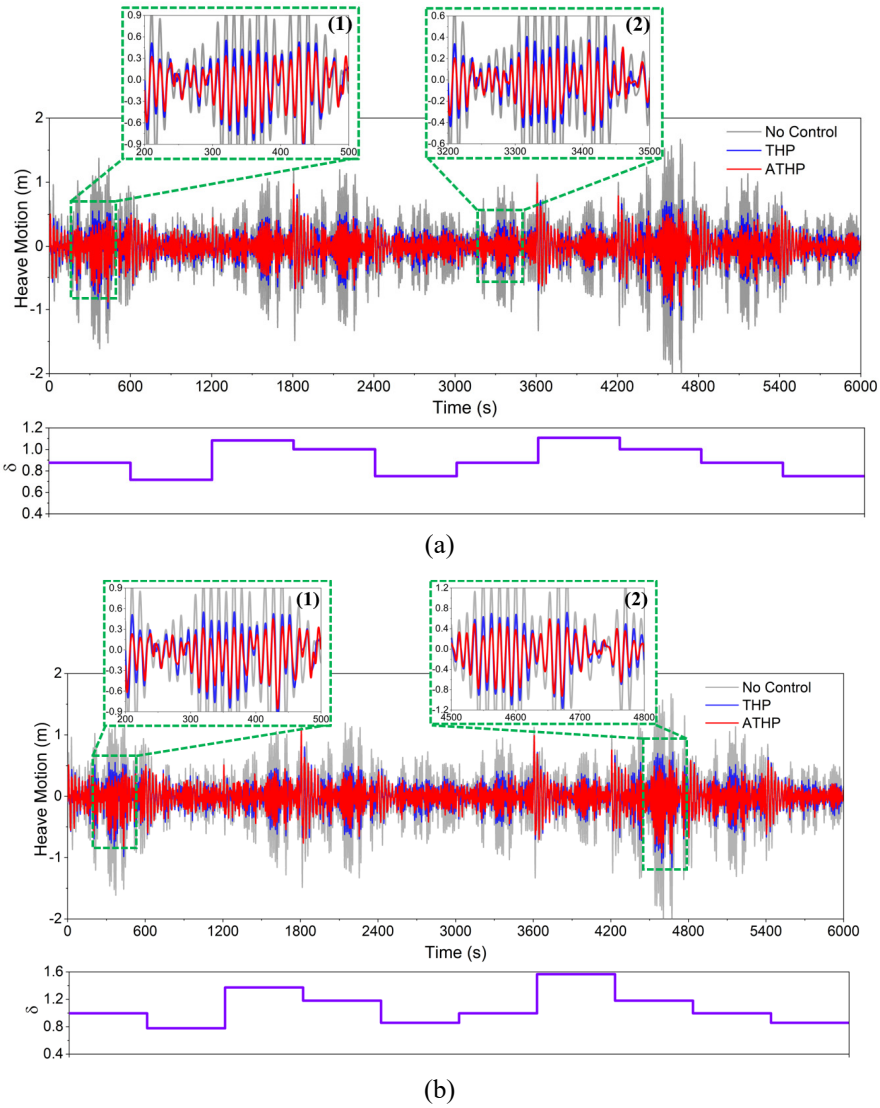

Fig. 17 Heave motion time histories of the SSP controlled by ATHP and time-varying inertance-to-mass ratio of ATHP. (a) J_1 optimization; (b) J_2 optimization

figure). For comparison purposes, the heave responses of the uncontrolled SSP and SSP-THP are also presented in the figure as well. In addition, some partially enlarged views are also added in Fig. 17 to illustrate the control performance of ATHP more clearly. Some general conclusions can be drawn from the results: (1) the heave responses of the SSP-ATHP and SSP-THP systems are effectively suppressed compared to those of the uncontrolled SSP; (2) the ATHP shows better control performance than the conventional THP; (3) both J_1 and J_2 optimizations are valid to obtain the optimum inertance-to-mass ratio of ATHP. To quantitatively evaluate the control performance of ATHP, the root-mean-square (RMS) values of heave motion are further calculated, and Table 6 tabulates the results. As listed, the heave motion RMS of the uncontrolled SSP is 0.438 m, which is reduced by 46.42% when the conventional THP is used. As for the J_1-optimized and J_2-optimized ATHPs, they reduce the heave motion RMS by 52.71% and 53.11%, respectively, compared to the uncontrolled SSP. Moreover, the reduction ratios are also

Table 6 Heave motion RMS of the SSP with different control systems

Optimizations	RMS (m)			Reduction ratio (%)
	No control	THP	ATHP	
J_1	0.438	0.235	0.207	11.73
J_2	0.438	0.235	0.205	12.48

calculated according to Eq. (24), and they are respectively 11.73% and 12.48% under J_1 and J_2 optimizations. It is worth mentioning that the reduction ratios listed in Table 6 are the performance improvement of ATHP over the entire time span (i.e., 6000 s shown in Fig. 17), and could be higher in some time ranges. For example, the reduction ratios of ATHP under J_1 and J_2 optimizations respectively reach 14.32% and 15.79% when the time range is 0~600 s. This phenomenon is due to the fact that the dominant wave frequency (corresponding to the wave peak period) varies with the time (see Fig. 16), and the ATHP has different

performance improvements at different wave peak periods as shown in Fig. 11.

6. Conclusions

In this study, an adaptive tuned heave plate (ATHP) is developed based on inerter, which allows to overcome the limitation of the conventional THP and realize adaptation to the real-time wave. The analytical model of SSP-ATHP is established and equilibrium equations of motion are formulated. Two optimization strategies (namely J_1 and J_2 optimizations) are adopted to obtain the optimum inertance-to-mass ratio of ATHP. The frequency-domain control effectiveness of ATHP is then investigated and compared to those of the uncontrolled SSP and SSP-THP systems. Parametric analyses are systematically performed to assess the influences of the pre-specified frequency ratio, pre-specified damping ratio, heave plate sizes, wave peak periods and heights on the control effectiveness of ATHP. In addition, a Simulink model is also constructed to investigate the control effectiveness of ATHP in the time domain. Conclusions are presented as follows:

The proposed ATHP can adaptively adjust its optimum inertance-to-mass ratio by tracking the real-time peak period of wave and shows better control performance than the conventional THP. Compared to the conventional THP, the ATHP in the present study can further improve the control performance by more than 11% in the time domain.

The pre-specified frequency and damping ratios can significantly affect the optimum inertance-to-mass ratio and control effectiveness of ATHP, and the optimum inertance-to-mass ratio of ATHP is more sensitive to the variation of the pre-specified frequency ratio.

The heave plate size has a marginal influence on the optimum inertance-to-mass ratio of ATHP but a significant influence on the control performance of ATHP. A larger heave plate size can result in a bigger reduction ratio.

The wave peak period can strongly affect the optimum inertance-to-mass ratio and control performance of ATHP. Compared to the wave peak period, the influences of wave height on the optimum inertance-to-mass ratio and control performance of ATHP are very limited.

Acknowledgments

This research was supported financially by the National Natural Science Foundation of China (No. 52208452) and China Postdoctoral Science Foundation (No. 2022M710283), which are gratefully appreciated.

References

Ali Sadeghian, M., Yang, J., Wang, X.E. and Wang, F. (2021), "Novel adaptive tuned viscous inertance damper (ATVID) with adjustable inertance and damping for structural vibration control", *Structures*, **29**, 814-822. https://doi.org/10.1016/j.istruc.2020.11.050

Alujević, N., Čakmak, D., Wolf, H. and Jokić, M. (2018), "Passive and active vibration isolation systems using inerter", *J. Sound Vib.*, **418**, 163-183. https://doi.org/10.1016/j.jsv.2017.12.031.

Asami, T., Nishihara, O. and Baz, A.M. (2002), "Analytical solutions to H_∞ and H_2 optimization of dynamic vibration absorbers attached to damped linear systems", *J. Vib. Acoust.*, **124**(2), 284-295. https://doi.org/10.1115/1.1456458.

Berardengo, M., Cigada, A., Guanziroli, F. and Manzoni, S. (2015), "Modelling and control of an adaptive tuned mass damper based on shape memory alloys and eddy currents", *J. Sound Vib.*, **349**, 18-38. https://doi.org/10.1016/j.jsv.2015.03.036

Brzeski, P., Lazarek, M. and Perlikowski, P. (2017), "Experimental study of the novel tuned mass damper with inerter which enables changes of inertance", *J. Sound Vib.*, **404**, 47-57. https://doi.org/10.1016/j.jsv.2017.05.034

Chakrabarti, S.K. (1987), *Hydrodynamics of offshore structures*: WIT Press, Southampton, UK.

Cummins, W. (1962), "The impulse response function and ship motions", *Schiffstechnik*, **9**, 101-109.

Det Norske Veritas (2011), *Modelling and analysis of marine operations*, Det Norske Veritas, Olso, Norway.

Faltinsen, O. (1993), *Sea loads on ships and offshore structures*: Cambridge University Press, Cambridge, UK.

Hu, Y., Wang, J., Chen, M.Z.Q., Li, Z. and Sun, Y. (2018), "Load mitigation for a barge-type floating offshore wind turbine via inerter-based passive structural control", *Eng. Struct.*, **177**, 198-209. https://doi.org/10.1016/j.engstruct.2018.09.063

Huang, H., Mosalam, K.M. and Chang, W.-S. (2020), "Adaptive tuned mass damper with shape memory alloy for seismic application", *Eng. Struct.*, **223**. https://doi.org/10.1016/j.engstruct.2020.111171

Ikago, K., Saito, K. and Inoue, N. (2012), "Seismic control of single-degree-of-freedom structure using tuned viscous mass damper", *Earthq. Eng. Struct. Dyn.*, **41**(3), 453-474. https://doi.org/10.1002/eqe.1138

Javidialesaadi, A. and Wierschem, N.E. (2019), "An inerter-enhanced nonlinear energy sink", *Mech. Syst. Signal Process.*, **129**, 449-454. https://doi.org/10.1016/j.ymssp.2019.04.047

Kim, H.S. and Kang, J.W. (2012), "Semi-active fuzzy control of a wind-excited tall building using multi-objective genetic algorithm", *Eng. Struct.*, **41**, 242-257. https://doi.org/10.1016/j.engstruct.2012.03.038

Lazar, I., Neild, S. and Wagg, D. (2014), "Using an inerter-based device for structural vibration suppression", *Earthq. Eng. Struct. Dyn.*, **43**(8), 1129-1147. https://doi.org/10.1002/eqe.2390

Li, B., Huang, Z., Low, Y.M. and Ou, J. (2013), "Experimental and numerical study of the effects of heave plate on the motion of a new deep draft multi-spar platform", *J. Mar. Sci. Tech.*, **18**(2), 229-246. https://doi.org/10.1007/s00773-012-0203-0

Liu, K. and Ou, J. (2016), "A novel tuned heave plate system for heave motion suppression and energy harvesting on semi-submersible platforms", *Sci. China Technol. Sci.*, **59**(6), 897-912. https://doi.org/10.1007/s11431-016-6055-9

Lu, Z., Zhang, J. and Wang, D. (2021), "Energy analysis of particle tuned mass damper systems with applications to MDOF structures under wind-induced excitation", *J. Wind. Eng. Ind. Aerodyn.*, **218**, 104766. https://doi.org/10.1016/j.jweia.2021.104766

Ma, R., Bi, K. and Hao, H. (2018), "Mitigation of heave response of semi-submersible platform (SSP) using tuned heave plate inerter (THPI)", *Eng. Struct.*, **177**, 357-373. https://doi.org/10.1016/j.engstruct.2018.09.085

Ma, R., Bi, K. and Hao, H. (2019), "A novel rotational inertia damper for heave motion suppression of semisubmersible platform in the shallow sea", *Struct. Control Health Monitor.*, **26**(7), e2368. https://doi.org/10.1002/stc.2368

Ma, R., Bi, K. and Hao, H. (2020), "Heave motion mitigation of semi-submersible platform using inerter-based vibration isolation system (IVIS)", *Eng. Struct.*, **219**, 110833. https://doi.org/10.1016/j.engstruct.2020.110833

Ma, R., Bi, K. and Hao, H. (2021a), "Inerter-based structural vibration control: A state-of-the-art review", *Eng. Struct.*, **243**, 112655. https://doi.org/10.1016/j.engstruct.2021.112655

Ma, R., Bi, K. and Hao, H. (2021b), "A novel rotational inertia damper for amplifying fluid resistance: Experiment and mechanical model", *Mech. Syst. Signal Process.*, **149**, 107313. https://doi.org/10.1016/j.ymssp.2020.107313

Ma, R., Bi, K. and Hao, H. (2021c), "Wave flume tests of a semi-submersible platform controlled by a novel rotational inertia damper", *Ocean Eng.*, **238**, 109718. https://doi.org/10.1016/j.oceaneng.2021.109718

Marian, L. and Giaralis, A. (2014), "Optimal design of a novel tuned mass-damper–inerter (TMDI) passive vibration control configuration for stochastically support-excited structural systems", *Probabilistic Eng. Mech.*, **38**, 156-164. https://doi.org/10.1016/j.probengmech.2014.03.007

Nagarajaiah, S. and Jung, H.J. (2014), "Smart tuned mass dampers: recent developments", *Smart Struct. Syst., Int. J.*, **13**(2), 173-176. https://doi.org/10.12989/sss.2014.13.2.173

Nakamura, Y., Fukukita, A., Tamura, K., Yamazaki, I., Matsuoka, T., Hiramoto, K. and Sunakoda, K. (2014), "Seismic response control using electromagnetic inertial mass dampers", *Earthq. Eng. Struct. Dyn.*, **43**(4), 507-527. https://doi.org/10.1002/eqe.2355

Newman, J.N. and Landweber, L. (1978), *Marine hydrodynamics*, MIT Press, Cambridge, UK.

Perez, T. and Fossen, T.I. (2009), "A matlab toolbox for parametric identification of radiation-force models of ships and offshore structures", *Model, Identif. Control*, **30**(1), 1-15. https://doi.org/10.4173/mic.2009.1.1

Petrini, F., Giaralis, A. and Wang, Z. (2020), "Optimal tuned mass-damper-inerter (TMDI) design in wind-excited tall buildings for occupants' comfort serviceability performance and energy harvesting", *Eng. Struct.*, **204**, 109904. https://doi.org/10.1016/j.engstruct.2019.109904

Pietrosanti, D., De Angelis, M. and Basili, M. (2017), "Optimal design and performance evaluation of systems with Tuned Mass Damper Inerter (TMDI)", *Earthq. Eng. Struct. Dyn.*, **46**(8), 1367-1388. https://doi.org/10.1002/eqe.2861

Rong, K. and Lu, Z. (2021), "Performance of a gas-spring tuned mass damper under seismic excitation", *Struct. Eng. Mech., Int. J.*, **80**(2), 157-168. https://doi.org/10.12989/sem.2021.80.2.157

Sarkar, S. and Fitzgerald, B. (2022), "Fluid inerter for optimal vibration control of floating offshore wind turbine towers", *Eng. Struct.*, **266**, 114558. https://doi.org/10.1016/j.engstruct.2022.114558

Smith, M.C. (2002), "Synthesis of mechanical networks: the inerter", *IEEE Trans. Automat. Contr.*, **47**(10), 1648-1662. https://doi.org/10.1109/TAC.2002.803532

Song, J., Bi, K., Xu, K., Han, Q. and Du, X. (2021), "Seismic responses of adjacent bridge structures coupled by tuned inerter damper", *Eng. Struct.*, **243**. https://doi.org/10.1016/j.engstruct.2021.112654

Stewart, G.M. and Lackner, M.A. (2014), "The impact of passive tuned mass dampers and wind–wave misalignment on offshore wind turbine loads", *Eng. Struct.*, **73**, 54-61. https://doi.org/10.1016/j.engstruct.2014.04.045

Sun, T. and Zhang, Z. (2022), "Optimal control and performance evaluation of an inerter-based point absorber wave energy converter", *Ocean Eng.*, **259**, 111883. https://doi.org/10.1016/j.oceaneng.2022.111883

Sun, C., Nagarajaiah, S. and Dick, A. (2014), "Family of smart tuned mass dampers with variable frequency under harmonic excitations and ground motions: closed-form evaluation", *Smart Struct. Syst., Int. J.*, **13**(2), 319-341. https://doi.org/10.12989/sss.2014.13.2.319

Tao, L. and Cai, S. (2004), "Heave motion suppression of a Spar with a heave plate", *Ocean Eng.*, **31**(5-6), 669-692. https://doi.org/10.1016/j.oceaneng.2003.05.005

Wang, Y., Lynch, J.P. and Law, K.H. (2007), "A wireless structural health monitoring system with multithreaded sensing devices: design and validation", *Struct. Infrastruct. Eng.*, **3**(2), 103-120. https://doi.org/10.1080/15732470600590820

Wang, Z., Gao, H., Wang, H. and Chen, Z. (2018), "Development of stiffness-adjustable tuned mass dampers for frequency retuning", *Adv. Struct. Eng.*, **22**(2), 473-485. https://doi.org/10.1177/1369433218791356

Weber, F. and Maślanka, M. (2012), "Frequency and damping adaptation of a TMD with controlled MR damper", *Smart Mater. Struct.*, **21**(5). https://doi.org/10.1088/0964-1726/21/5/055011

Xu, T., Liang, M., Li, C. and Yang, S. (2015), "Design and analysis of a shock absorber with variable moment of inertia for passive vehicle suspensions", *J. Sound Vib.*, **355**, 66-85. https://doi.org/10.1016/j.jsv.2015.05.035

Xu, K., Bi, K., Ge, Y., Zhao, L., Han, Q. and Du, X. (2020), "Performance evaluation of inerter-based dampers for vortex-induced vibration control of long-span bridges: A comparative study", *Struct. Control Health Monit.*, **27**(6), e2529. https://doi.org/10.1002/stc.2529

Zhang, Chen, Z., Hua, X., Huang, Z. and Niu, H. (2020), "Design and dynamic characterization of a large-scale eddy current damper with enhanced performance for vibration control", *Mech. Syst. Signal Process.*, **145**, 106879. https://doi.org/10.1016/j.ymssp.2020.106879

Zhao, Z., Zhang, R., Jiang, Y. and Pan, C. (2019), "A tuned liquid inerter system for vibration control", *Int. J. Mech. Sci.*, **164**, 105171. https://doi.org/10.1016/j.ijmecsci.2019.105171

Zhu, H., Li, Y., Shen, W. and Zhu, S. (2019), "Mechanical and energy-harvesting model for electromagnetic inertial mass dampers", *Mech. Syst. Signal Process.*, **120**, 203-220. https://doi.org/10.1016/j.ymssp.2018.10.023

HJ